PHYSICAL REVIEW B VOLUME 51, NUMBER 12 15 MARCH 1995-II

Extended Hubbard model with off-site interactions: Two-particle spectrum and Auger line shapes

C. Verdozzi
Interdisciplinary Research Centre in Surface Science, The University of Liverpool, P.O. Box 147, Liverpool L69 3BX, United Kingdom

M. Cini
Dipartimento di Fisica, Universitá di Roma II, Via della Ricerca Scientifica, I-00173 Roma, Italy
(Received 28 June 1994; revised manuscript received 29 November 1994)

We present a method for calculating the Green's function of two particles on a periodic lattice, with arbitrary distance-dependent interactions (extended Hubbard model). We develop the exact results together with their dispersionless limit (local approximation) for the sake of comparison. Numerical calculations for a repulsive, Thomas-Fermi-like potential illustrate the effects of including off-site interactions in a simple cubic lattice. For strong correlations, the spectrum differs qualitatively from that of the Hubbard model, and may show several resonant states instead of just one. The formalism lends itself to many physical applications: here, we discuss its consequences for the theory of Auger core-valence-valence line shapes of solids. We show that Auger spectroscopy is a method for measuring the strength of electron-electron interactions, both on site and off site.

I. INTRODUCTION

In recent years, the Hubbard model[1] has been subject to a renewed attention for its relevance for high-T_c superconductivity, quantum antiferromagnetism, and ferromagnetism, thus playing a central role in theoretical investigations of strongly correlated systems. Besides the above fundamental issues, the Hubbard model is also used as a theoretical framework of some spectroscopic processes when, under the perturbing action of the probe, part of the electronic degrees of freedom in the sample exhibits an interplay between itinerant and localized behavior.

In its simplest form, the Hubbard model (HM) consists of a single-band tight-binding Hamiltonian, plus a periodic, on-site, interaction term U, which accounts for the dominant part of the Coulomb repulsion experienced by the electrons. The long-range part of the potential is neglected, and one is left only with the on-site interaction terms. Adding off-site interaction terms, we obtain an extended Hubbard model (EHM). To what extent the inclusion of off-site terms is relevant to the description of strongly correlated systems is a matter of current debate in the literature, and the general issue is a difficult one. On the other hand, exact results of two- (or few-) body problems on an infinite lattice are often of interest because they are known to be preliminary to the study of the related, much more involved, many-body problem. In this respect, for the HM the prototype exact result is the Kanamori[2] solution for the two-body problem.

Working out the eigenvalue problem numerically is the most direct way to the exact solution. For example, a diagonalization technique which makes use of Löwdin's partitioning method has recently been used[3] to include intercell interaction in the theory of Auger spectra from polymeric chains. Also, Navarro and Wang[4] have recently introduced an implemented diagonalization method for the EHM solution of a dilute (few particles) system.

If one is not interested in as much detail as is contained in the single eigenvalue/eigenvector, Green's functions are the usual shortcut to provide more compact information such as, for example, the density of states. Accordingly, we present here a Green's function method for the solution of a two-particle EHM, and investigate the effect of off-site interactions on the density of states. The method (valid for arbitrary dimension, lattice, and interaction) bypasses diagonalization techniques and gives directly the interacting two-particle Green's function, in terms of noninteracting propagators. It extends to the case of two particles the approach introduced by Callaway and Hughes[5] for a cluster of impurities in a lattice, and we believe that it has a number of potential applications. An obvious occurrence of a two-body EHM problem arises in the theory of Frenkel excitons,[6] where the interaction is attractive. However, the case of Frenkel excitons is deferred to future work, because electron and hole must belong to different bands. Below we shall concentrate on the simpler case of Auger core-valence-valence (CVV) line shapes,[7] where the need for an extension of the Hubbard model has been recognized only recently. This is of some general interest because it allows the direct observation and measurement of the interparticle interaction strength in the valence bands of solids, and their distance dependence.

The acronym CVV is used for those Auger transitions that produce two holes in valence states. The basic theoretical framework for these transitions was introduced by Cini[8] and Sawatzky,[9] and is referred to as Cini-Sawatzky theory (CST) in the literature. Typically, intra-atomic Auger processes (where the primary core hole and final-state holes belong to the same atom) dominate, while interatomic transition rates are smaller by orders of magnitude. Thus two holes are created at one site of the lattice. Complications arise in partially filled bands, which polarize around the primary hole, leading to many-body effects;[10] however, in completely filled

0163-1829/95/51(12)/7412(9)/$06.00

bands, all that remains is a two-hole process. Therefore the line shape of solids with completely filled bands depends on the local density of states of the two final-state holes, which are created on one atom, where they repel each other strongly, and may subsequently delocalize into the crystal. In this paper, we specialize to the case of filled bands.

In this case, CST is based on exact solutions of two-body problems for an Anderson Hamiltonian[11,8] and a Hubbard model,[1,2,9] and the relationship between the two formulations has been examined.[12,13] With an appropriate account of multiplet effects,[14] the CST was adequate until recently the improved resolution and a more accurate energy referencing of the experiments allowed the observation of small but interesting discrepancies,[15] which apparently can be rationalized with off-site interactions.[16,17] Thus here we apply our EHM Green's function solution to Auger CVV transitions from filled bands.

We state now the plan of the paper. In Sec. II we describe our mathematical approach, that for a two-body EHM problem. In Sec. III we discuss the general properties of the solution, by using a simple cubic lattice as a numerical test case, and the relevance of off-site interactions to the theory of Auger spectroscopy, in the light of current theoretical treatments and recent experimental evidence. Finally, we report in Sec. IV our concluding remarks and directions for future work.

II. FORMALISM

A. Two-particle Green's function

We allow for a general interaction V(r) and consider the extended Hubbard model:

$$H=\sum_{ks} E(\mathbf{k})n_{ks}+\sum_{Rr} V(r)n_{R\uparrow}n_{R+r\downarrow} , \tag{1}$$

where $E(\mathbf{k})$ are the Bloch energies of a nondegenerate band, $n_{ks}=a^{\dagger}_{ks}a_{ks}$, $n_{Rs}=a^{\dagger}_{Rs}a_{Rs}$ with s and **R** spin and site labels, respectively. We give a convenient and exact general method to determine the interacting two-particle Green's function

$$G_{R_1R_2R_3R_4}(z=E-i0^+)=\left\langle \mathbf{R}_1\uparrow,\mathbf{R}_2\downarrow \left| \frac{1}{z-H} \right| \mathbf{R}_3\uparrow,\mathbf{R}_4\downarrow \right\rangle . \tag{2}$$

We rewrite the interaction terms as

$$\sum_{Rr} V(r)|\mathbf{R}\uparrow,\mathbf{R}+\mathbf{r}\downarrow\rangle\langle\mathbf{R}\uparrow,\mathbf{R}+\mathbf{r}\downarrow| ,$$

where **r** describes the relative motion of the two particles and belongs to the lattice of relative motion, which we call the **r** lattice. Next, we go to an excitoniclike picture: omitting spin labels, we introduce

$$|\mathbf{R},\mathbf{R}+\mathbf{r}\rangle=N^{-1/2}\sum_{Q} e^{-iQ\cdot(R+r/2)}|\mathbf{Q},\mathbf{r}\rangle , \tag{3a}$$

where $N\to\infty$ is the number of sites, and

$$|\mathbf{Q},\mathbf{r}\rangle=e^{iQ\cdot r/2}(N)^{-1/2}\sum_{q} e^{-iq\cdot r}|\mathbf{Q}-\mathbf{q},\mathbf{q}\rangle . \tag{3b}$$

In the $|\mathbf{Q},\mathbf{r}\rangle$ basis, the Hamiltonian takes the form

$$H=\sum_{Q} H^{Q}, \quad H^{Q}=H_0^{Q}+H_1^{Q} \tag{4}$$

where

$$H_0^{Q}=\sum_{rr'} |\mathbf{Q},\mathbf{r}\rangle W^{Q}_{rr'}\langle\mathbf{Q},\mathbf{r}'| , \tag{5a}$$

with

$$W^{Q}_{rr'}=e^{-iQ\cdot(r-r')/2}\frac{1}{N}\sum_{q} e^{iq\cdot(r-r')}[E(\mathbf{Q}-\mathbf{q})+E(\mathbf{q})] \tag{5b}$$

and

$$H_1^{Q}=\sum_{r} V(\mathbf{r})|\mathbf{Q},\mathbf{r}\rangle\langle\mathbf{Q},\mathbf{r}| . \tag{6}$$

Due to translational symmetry, the most general two-particle Green's function can be written as

$$\left\langle 0,0+\mathbf{r}\left|\frac{1}{z-H}\right|\mathbf{R},\mathbf{R}+\mathbf{r}'\right\rangle=\frac{1}{N}\sum_{Q} e^{-iQ\cdot R}e^{iQ\cdot(r-r')/2}\times G^{Q}_{rr'}(z) , \tag{7}$$

where

$$G^{Q}_{rr'}(z)=\left\langle \mathbf{Q},\mathbf{r}\left|\frac{1}{z-H^{Q}}\right|\mathbf{Q},\mathbf{r}'\right\rangle . \tag{8}$$

To proceed, we consider the chain of operator identities

$$\frac{1}{\omega-H^{Q}}=\frac{1}{\omega-H_0^{Q}}+\frac{1}{\omega-H_0^{Q}}V\frac{1}{\omega-H^{Q}}$$

$$=\frac{1}{\omega-H_0^{Q}}+\frac{1}{\omega-H_0^{Q}}V\left[\frac{1}{\omega-H_0^{Q}}+\frac{1}{\omega-H^{Q}}V\frac{1}{\omega-H_0^{Q}}\right]=\frac{1}{\omega-H_0^{Q}}+\frac{1}{\omega-H_0^{Q}}\left[V+V\frac{1}{\omega-H^{Q}}V\right]\frac{1}{\omega-H_0^{Q}} . \tag{9}$$

We expand the inverse operator inside the large parentheses, and summing the geometric series, we end up with

$$\frac{1}{\omega-H^{Q}}=\frac{1}{\omega-H_0^{Q}}+\frac{1}{\omega-H_0^{Q}}\frac{1}{1-V[1/(\omega-H_0^{Q})]}V\frac{1}{\omega-H_0^{Q}} . \tag{10}$$

By taking matrix elements on the $|\mathbf{Q},\mathbf{r}\rangle$ basis, we eventually get

$$G^{\mathbf{Q}}_{\mathbf{rr}'}(z)=g^{\mathbf{Q}}_{\mathbf{rr}'}(z)+\Lambda^{\mathbf{Q}}_{\mathbf{rr}'}(z)\ , \tag{11}$$

where $g^{\mathbf{Q}}_{\mathbf{rr}'}$ is given by Eq. (8) for $H^{\mathbf{Q}}_1=0$, and

$$\Lambda^{\mathbf{Q}}_{\mathbf{rr}'}(z)=\sum_{ij} g^{\mathbf{Q}}_{\mathbf{ri}}(z)\left[\frac{\mathbb{1}}{\mathbb{1}-\mathbf{M}^{\mathbf{Q}}(z)}\right]_{ij} V(j)g^{\mathbf{Q}}_{\mathbf{jr}'}(z)\ . \tag{12}$$

Here, $\mathbb{1}$ is the unit matrix and

$$[\mathbf{M}^{\mathbf{Q}}(z)]_{\mathbf{rr}'}=V(\mathbf{r})g^{\mathbf{Q}}_{\mathbf{rr}'}(z)\ . \tag{13}$$

Equations (11)–(13) solve the problem; they are formally similar to the equations which describe the motion of a single particle on a lattice in the presence of a cluster of impurities. We see that the size of the computation does not depend on the physical size of the crystal, but on the range of the potential. The present approach is particularly useful if V is short ranged, because then we may solve for the two-hole dynamics in an infinite system by performing a matrix inversion in a small interaction cluster in the **r** lattice. It is interesting to note that if the interaction cluster is finite, we may rephrase all the two-body problems exactly as if the motion were confined, in terms of a non-Hermitian effective Hamiltonian. This is shown in the Appendix.

B. Use of symmetry

Point symmetry can reduce the size of the inversion problem associated with **M**. We illustrate this by choosing a special case of Eq. (7), namely,

$$\left\langle 0,0\left|\frac{1}{z-H}\right|\mathbf{R},\mathbf{R}+\mathbf{r}\right\rangle=\frac{1}{N}\sum_{\mathbf{Q}} e^{-i\mathbf{Q}\cdot\mathbf{R}}e^{-i\mathbf{Q}\cdot\mathbf{r}/2}G^{\mathbf{Q}}_{0\mathbf{r}}(z)\ , \tag{14a}$$

$$G^{\mathbf{Q}}_{0\mathbf{r}}(z)=\left\langle \mathbf{Q},0\left|\frac{1}{z-H^{\mathbf{Q}}}\right|\mathbf{Q},\mathbf{r}\right\rangle\ . \tag{14b}$$

The two-particle Green's function in Eqs. (14) is sufficient in many situations (e.g., for exciton recombination and for Auger spectroscopy of closed bands).

The relative motion of the two particles takes place in a lattice that we called the **r** lattice. The **r** lattice is identical to the Bravais lattice of the crystal; however, the Hamiltonian $H^{\mathbf{Q}}_0$ which describes the noninteracting particles in the $|\mathbf{Q},\mathbf{r}\rangle$ basis has a **Q**-dependent point symmetry, which is generally reduced. Actually, for fixed **Q**, $H^{\mathbf{Q}}_0$ describes the motion of one effective particle (of coordinate **r**) in a distorted lattice, which we call the **Q** lattice. It is this reduced symmetry that we can still exploit. The **Q** lattice can be partitioned in terms of successive shells $\{n\}$ of symmetry related sites. For any **Q**, the state $|\mathbf{Q},0\rangle$ is total symmetric, i.e., it belongs to the irreducible representation Γ_0 of $H^{\mathbf{Q}}_0$. Accordingly, the power expansion of $\Lambda^{\mathbf{Q}}_{0\mathbf{r}}(z)$ connects only total-symmetric states to $|\mathbf{Q},0\rangle$. Therefore we introduce yet another lattice, called the equivalent lattice, with sites which are totally symmetric combinations of those of the **Q** lattice, namely,

$$|i\rangle\equiv|\mathbf{Q},i\rangle=N_i^{-1/2}\sum_{\mathbf{r}_i\in\text{ shell }i}|\mathbf{Q},\mathbf{r}_i\rangle\ , \tag{15}$$

and we denote them by italic site indices. A cluster in the **Q** lattice has an equivalent cluster with many fewer sites, where Eq. (11), with italic indices, still applies. We may write

$$\Lambda^{\mathbf{Q}}_{0r}(z)=\sum_{ij} g^{\mathbf{Q}}_{0i}(z)\left[\frac{\mathbb{1}}{\mathbb{1}-\mathbf{M}^{\mathbf{Q}}(z)}\right]_{ij} V_j g^{\mathbf{Q}}_{jr}(z)\ , \tag{16}$$

with

$$\mathbf{M}^{\mathbf{Q}}_{mn}(z)=V_m g^{\mathbf{Q}}_{mn}(z)\ , \tag{17}$$

where $V_i=V(\mathbf{r}_i)$ for any r_i in shell i. Of course, $|\mathbf{Q},0\rangle=|\mathbf{Q},\mathbf{0}\rangle$. Although we have exemplified the use of symmetry in a special case of Eq. (7), the same technique can be applied in general.

C. Simple cubic lattice

We wish to show the method by a detailed discussion of the local two-particle Green's function of cubium:

$$G_L(z)=\frac{1}{N}\sum_{\mathbf{Q}} G^{\mathbf{Q}}_{00}(z)=\frac{1}{N}\sum_{\mathbf{Q}}\left\langle \mathbf{Q},0\left|\frac{1}{z-H^{\mathbf{Q}}}\right|\mathbf{Q},0\right\rangle\ . \tag{18}$$

The relevant Bloch energies of Eq. (1) are

$$E(\mathbf{k})=\cos(k_x a)+\cos(k_y a)+\cos(k_z a)\ . \tag{19}$$

In Eq. (19), a is the lattice parameter, the site energy is set equal to zero, and all energies are measured in units of $2\mathcal{V}$, where $\mathcal{V}$ is the nearest-neighbor hopping parameter. The propagators $g^{\mathbf{Q}}_{ij}(z)$ in Eqs. (16) and (17) are linear combinations of ordinary Green's functions $g^{\mathbf{Q}}_{\mathbf{r}_i\mathbf{r}_j}=g^{\mathbf{Q}}_{\mathbf{r}_i-\mathbf{r}_j;0}$ of the **Q** lattice, where $\mathbf{r}_i,\mathbf{r}_j$ belong to shells i and j, respectively, and translational symmetry has been used. By expressing $\mathbf{r}_i-\mathbf{r}_j$ in terms of **Q**-lattice coordinates *lmn*, the generic Green's function is

$$g^{\mathbf{Q}}(lmn;z=E-i0^+)=\frac{1}{\pi^3}\int_0^\pi dx\,dy\,dz\frac{\cos(lx)\cos(my)\cos(nz)}{z-\gamma_x\cos x-\gamma_y\cos y-\gamma_z\cos z}\ , \tag{20}$$

where $\gamma_i=2\cos(\mathbf{Q}_i a/2)$. Alternatively, in terms of Bessel functions,

$$g^{\mathbf{Q}}(lmn;z)=(i)^{l+m+n+1}\int_0^\infty dt\,e^{-i(E-i0^+)t}J_l(\gamma_x t)\times J_m(\gamma_y t)J_n(\gamma_z t)\ . \tag{21}$$

Equations (20) and (21) show explicitly that **Q** (or γ) fixes the symmetry:[18] (I) orthorhombic ($\gamma_x\neq\gamma_y\neq\gamma_z$), (II) tetragonal ($\gamma_x\neq\gamma_y=\gamma_z$), (III) cubic ($\gamma_x=\gamma_y=\gamma_z$). The convenience of the equivalent cluster can be easily illustrated by a specific example: if V(r) has spherical symmetry, and $V(r>2a)=0$, direct use of Eqs. (12) and (13) would require the inversion of a 33×33 matrix, while by using symmetry, the matrix is 11×11 for (I), 8×8 for (II), and 5×5 for (III). For each of cases (I)–(III), by using the recurrence relation

$$-2\delta_{l0}\delta_{m0}\delta_{n0}+2zg^{Q}_{lmn}(z)=\gamma_x[g^{Q}_{l+1mn}(z)+g^{Q}_{l-1mn}(z)]+\gamma_y[g^{Q}_{lm+1n}(z)+g^{Q}_{lm-1n}(z)]+\gamma_z[g^{Q}_{lmn+1}(z)+g^{Q}_{lmn-1}(z)] , \quad (22)$$

the generic $g^{Q}(lmn;z)$ is given by an algebraic combination of $g^{Q}(l=0mn;z)$ and this reduces the number of independent Green's functions to be calculated. They are[18] 27 for (I), 19 for (II), and 5 for (III). In addition, we used the symmetry

$$g^{Q}(lmn,0;-E-i\Gamma)=(-1)^{l+m+n+1}\times[g^{Q}(lmn,0;E-i\Gamma)]^* \quad (23)$$

to obtain simultaneously g^{Q} at E and $-E$ values.

D. The Q integrals

The local two-particle Green's function $G_L(z)$, Eq. (18), requires a **Q** integration. This was approximated by a sum over 120 **Q** vectors in the irreducible ($\frac{1}{48}$) sector of the first Brillouin zone, according to the Chadi-Cohen method.[19] In the actual calculation, we set $z=E-i\Gamma$, with a small by finite Γ. This phenomenological broadening ensures fast and uniform numerical convergence of the integral of Eq. (21) and smooths the oscillations in the spectrum due to the finite **Q** sum.

We must check the accuracy of the approximate **Q** integral, especially when the integrand may develop bound states outside the continuum. To this end, we considered the following test Hamiltonian:

$$H=H_{TB}+\mathcal{U}n_{0+} , \quad (24)$$

where H_{TB} is a tight-binding Hamiltonian. In this rather artificial problem, the particles are independent. Thus the local two-particle Green's function is

$$G_L^{+-}=\frac{1}{2\pi i}S_{00}^{+}\otimes S_{00}^{-} , \quad (25)$$

where $S^{\pm}$ is the one-particle Green's function: for spin down, this is the same as for H_{TB},

$$S_{00}^{-}(z)=S_{00}^{TB}(z) , \quad (26)$$

while for spin up, it is Wolff-Clogston distorted:

$$S_{00}^{+}(z)=S_{00}^{TB}(z)[1-WS_{00}^{TB}(z)]^{-1} . \quad (27)$$

For a simple cubic lattice, $S_{00}^{TB}(z)$ is known analytically and G_L^{+-} can be found with Eq. (25) with no need for a **Q** integration. On the other hand, using

$$S_{00}^{TB}(z)=\frac{1}{N}\sum_{q}\frac{1}{z-E(q)} , \quad (28)$$

and the distributive property of convolutions, we get

$$G_L^{+-}(z)=\frac{1}{N}\sum_{q}\frac{S_{00}^{TB}(z-E(q))}{1-\mathcal{U}S_{00}^{TB}(z-E(q))} . \quad (29)$$

In Eq. (29) G_L^{+-} was evaluated by a finite (120 **Q** points) summation. The two different calculations of G_L^{+-} were in very good agreement, as shown in Fig. 1.

We did two additional checks: (i) we used the full algorithm for the two-particle Green's function based on Eqs. (18) and (21) also in the trivial case $V(r)=0$, and compared it to the numerical convolution of the noninteracting one-particle Green's function; (ii) we calculated the momenta of the interacting spectrum analytically up to third order and compared them to the numerical momenta. The results confirmed that the method is correct and accurate.

E. The dispersionless (local) limit

In certain physical problems, one needs to consider the electron-electron interaction only at one site; this may be due to the system being inhomogeneous, but in most cases the reason is that configurations with both particles at any other site have little weight. A case in point is the description of Auger CVV transitions, where the exact solution[8] based on the Anderson impurity model[11] (in which the two particles are taken to have a short-range interaction U at a single site) is often used as a local approximation for the Auger Hubbard model,[9] where an identical short-range interaction U is taken to exist on every site.

In the above spirit, in this section we wish to develop the local limit of our EHM exact solutions: as far as it applies, we can use the great simplifications inherent in

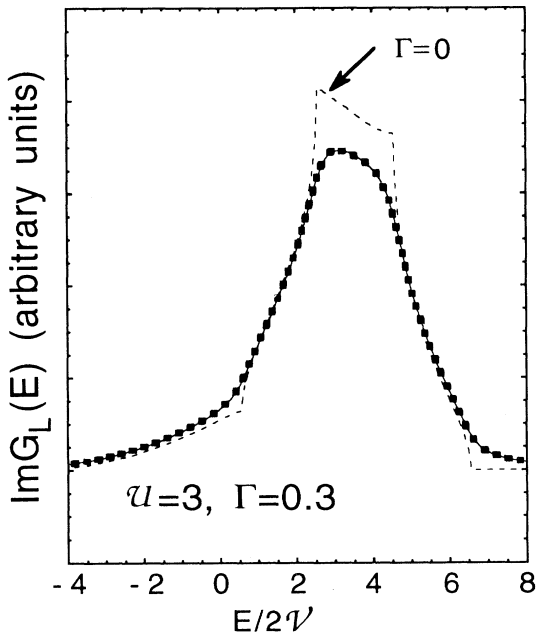

FIG. 1. Test of the accuracy of the truncated **Q** sum in Eqs. (29) for singular **Q** summands. The truncated **Q** sum is performed with 120 Chadi-Cohen **Q** points from $\frac{1}{48}$ of the first Brillouin zone. $\mathcal{U}=3$, $\Gamma=0.3$ in units of $2\mathcal{V}$, and $\mathcal{V}$ is the hopping term. Three curves are reported: dotted [Eq. (29), truncated **Q** sum, $\Gamma=0.3$], solid [Eq. (27), exact **Q** sum, $\Gamma=0.3$], and dashed [Eq. (27), exact **Q** sum, $\Gamma=0.0$]. The solid curve is obtained broadening the dashed curve.

the neglect of dispersion and avoid the demanding (especially for the multiple band case) **Q** summation of Eq. (18).

According to the definition of $g^{Q}_{rr'}(z)$ [Eq. (8) with $V=0$],

$$g^{Q}_{rr'}(z)=e^{-iQ\cdot(r-r')/2}\frac{1}{N}\sum_{q}\frac{e^{iq\cdot(r-r')}}{z-E(Q-q)-E(q)}$$
$$=e^{-iQ\cdot(r-r')/2}\frac{1}{N}\sum_{qq'}\frac{e^{iq\cdot(r-r')}\delta(q+q'-Q)}{z-E(q)-E(q')}\ . \tag{30}$$

The local approximation replaces $\delta(q+q'-Q)$ with its average value $1/N$, which yields

$$g^{Q}_{rr'}(z)\rightarrow\langle g_{rr'}(z)\rangle\equiv\frac{1}{2\pi i}S_{rr'}\otimes S_{00}\ ,$$

and employs Eqs. (11), (16), and (17) with $\langle g_{rr'}(z)\rangle$ in the place of $g^{Q}_{rr'}(z)$. The results will be discussed and compared to exact ones in the next section.

F. The case of parallel spins

The Hamiltonian of Eq. (1) is obviously *not* spin rotation invariant. The direct way to allow for this invariance is to replace (1) by

$$H=\sum_{ks}E(k)n_{ks}+\tfrac{1}{2}\sum_{Rss'}V(r)n_{Rs}n_{R+rs'}\ . \tag{31}$$

As far as a two particles with opposite spin are considered, Eq. (31) is identical to Eq. (1). However, Eq. (31) also describes the parallel spin case, which we turn to consider briefly. For the parallel spins, we split in Eq. (31) the $r=0$ terms from the $r\neq0$ ones; if $U=V(r=0)$, we have

$$H_{int}=\tfrac{1}{2}\sum_{Rs}Un_{Rs}+\tfrac{1}{2}\sum_{Rrs}^{r\neq0}V(r)n_{Rs}n_{R+rs}\ . \tag{32}$$

The first term in the right-hand side of Eq. (32) is a shift $U/2$ for the site energy, and consequently a shift U for the two-particle density of states. The other term in the right-hand side of Eq. (32) is the off-site interaction, for which we can essentially follow the above treatment, although the group theoretical analysis requires more algebra. There are a few, trivial, differences, due to the Pauli principle: G^{Q}_{00}, g^{Q}_{00}, vanish and the $g^{Q}_{rr'}$'s contain an exchange term; therefore in the interaction cluster the site $|Q,0\rangle$ is missing, i.e., we have a "punched" interaction.

Then, we recover many of the features of the above formal treatment. This is why we choose to explicitly describe the treatment of the antiparallel spin case: for opposite spin, there is a nontrivial competing behavior between $V(0)$ and $V(r\neq0)$, in affecting both the position and the line shape. For parallel spins the line shape depends solely on $V(r\neq0)$.

III. RESULTS AND DISCUSSION

The effect of the local term U on the two-particle local density of states is well known: as U increases, the shape of the two-particle local density of states is distorted, with the spectral weight being transferred to higher binding energies; for U exceeding a critical value U_{crit} (which depends on the type of lattice) a resonance develops out of the continuum, near the bottom of the two-particle band. The width of this resonance depends on the dispersive character of the bound state: for an impurity model,[8] with the on-site interaction retained at only one site (say site 0), the resonance is a δ function (zero width). For the periodic (Hubbard) model, the bound state can hop along the lattice, and the resonance has a finite dispersion width.[9] For both cases the position of the resonance is the same.[13] The impurity case can be thought of as the dispersionless limit of the homogeneous (periodic) one.[12] As the resonance develops, the spectral weight in the band region tends gradually to zero, for progressively higher U values. Now we turn to the effects of off-site interactions.

A. Model calculations

For illustration, we computed the diagonal Green's function

$$G_L(z)=\left\langle 0\uparrow0\downarrow\left|\frac{1}{z-H}\right|0\uparrow0\downarrow\right\rangle\ , \tag{33}$$

with a Thomas-Fermi-like potential up to two lattice distances:

$$V(r)=\begin{cases}U, & r=0\\ A\dfrac{e^{-(r/a)}}{(r/a)}, & 0<r\leq2a\\ 0 \quad \text{otherwise}\ .\end{cases} \tag{34}$$

We take the screening length equal to the lattice parameter a.

Let u be the nearest-neighbor interaction, $u=V(r=a)$. It is the single quantity that best characterizes the off-site strength of $V(r)$: a trivial example is $V(r)=u=\text{const}$, for $r\neq0$, with $V(0)=U$. In that case, one could calculate the spectrum by (i) distorting the noninteracting one by a strictly one-site term equal to $U-u$ and (ii) shifting the result by u. Therefore we prefer u rather than $A=ue$ as a label for our calculated spectra.

In the numerical calculations, the energy unit is $2\mathcal{V}$, with $\mathcal{V}$ the nearest-neighbor hopping parameter for the simple cubic lattice. In this way, for $V(r)=0$, the one-particle local density of states ranges from -3 to 3, the bandwidth is $W=6$, and the two-particle local density of states ranges from -6 to 6. In Table I, we report the values of U and u in the same units, for each of the four numerical cases we studied; the last column entries denote the corresponding figure. These particular choices of U and u will be useful in the next section.

In Figs. 2(a)–2(d), exact two-particle local densities of states (solid lines) are compared to their dispersionless limits (dashed). Figure 2(a), where $U=5.46$ and $u=2.84$, shows an intense peak close to the edge $E/2\mathcal{V}=6$ of the continuum, and a broader structure at lower binding en-

TABLE I. Values of U and u used for a comparison between exact and dispersionless limit solutions. The entries in the third column establish a correspondence between the U and u values and different panels in Fig. 2.

U	u	Fig.
5.46	2.84	2(a)
9.67	2.84	2(b)
9.74	4.7	2(c)
14.96	4.7	2(d)

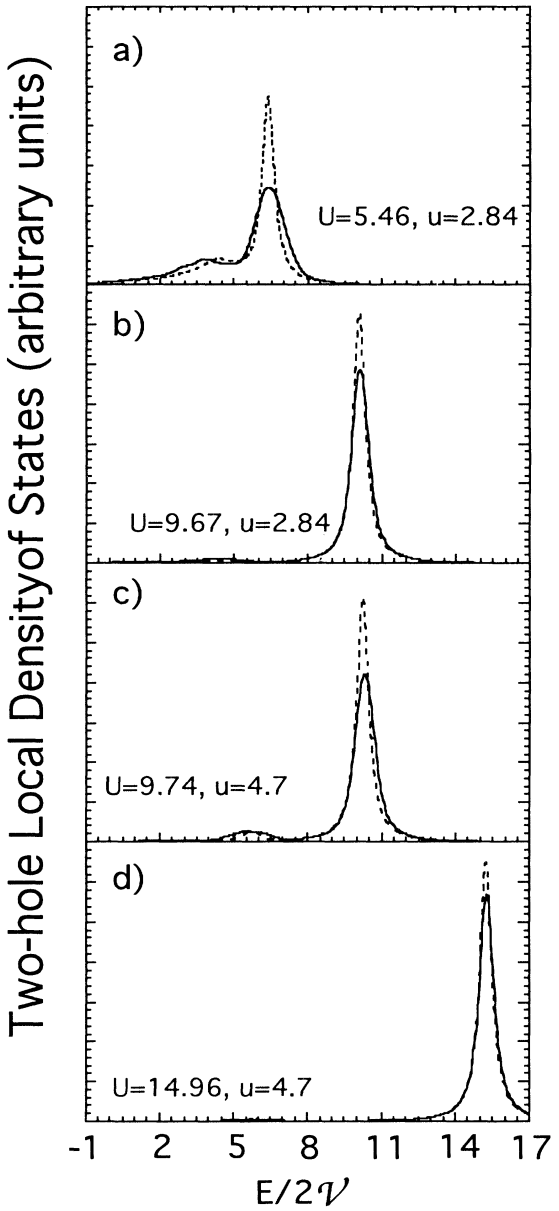

FIG. 2. Comparison between exact and dispersionless limit solutions for the two-particle local density of states in the presence of off-site interaction terms, for different U/W,u/W values. (See main text and Table I.) Energy units are the same as in Fig. 1. For all panels (a)–(d): solid line is the exact solution, dashed line is the dispersionless limit solution. In all cases $\Gamma=0.3$, $W=6$, and the edge of the continuum is at $E/2\mathcal{V}=6$.

ergy. The intense peak is the usual split-off resonance that is expected from the Hubbard model; the secondary peak is more interesting because it is due to a new bound state, although it falls in the continuum and gains some width from it. It disappears for $u=0$, leaving a very small bandlike residue, thus we may refer to the two structures as "the u peak," and "the U peak."

Thus with our choice of $V(\mathbf{r})$ we find two types of resonance. Pictorially, we may say that for each Q value, the solid behaves as a dimer, where one dimer site corresponds to two particles on the same lattice site, while the other represents two particles bound on two adjacent lattice sites. Evidently, the number of bound states depends on the range of the potential, and the Coulomb interaction will have infinitely many of them, in analogy with excitons. The above simple dimer picture will not apply with long-ranged potentials possessing a large number of bound states; it is then more appropriate to think of the two-particle resonance as a composite quasiparticle possessing a rich internal structure.

In going from Fig. 2(a) to Fig. 2(b), U increases and the u feature loses most of its weight: thus, if U is large enough to produce split-off states *and* $U \gg u$, we recover a single type of resonance. The wave function of the U bound state is dominated by configurations with the two particles on the same site, and gets an overwhelming overlap with $|0\uparrow 0\downarrow\rangle$.

Next, we compare the solid lines in Figs. 2(b) and 2(c). Since the U values are almost equal, the maxima approximately line up in energy. However, in Fig. 2(c), due to the larger off-site contribution $u=4.7$, the u peak is much more evident, and is becoming split off at $E/2\mathcal{V}\approx 6$. In Fig. 2(d), $u=4.7$ again, but u is much larger, and the U peak loses weight again.

A close look at the numerical results shows that U and u resonances have bonding and antibonding character, respectively: the U bound state slightly moves to higher binding energy with increasing u, but the u bound state moves to lower binding energy with increasing U.

The dispersionless limit of the theory (dashed curves) provides a fair approximation in all cases, reproducing both bound states and the main features of the exact solution. However, in Fig. 2(a), the exact curve has a larger intrinsic linewidth, and the dispersionless limit tends to concentrate the most prominent features in a smaller energy range. In Figs. 2(b)–2(d), there is less difference between the exact and dispersionless limit curves. This is due to the larger U values, which decrease the dispersive broadening.

For parallel spins, the interaction, if strong enough, can produce one (or more) resonances, but the maximum localization achievable is a nearest-neighbor localization. For the present model (which does not include band degeneracy) only the *u* peak would be expected to show up in the line shape.

B. Auger spectroscopy

This work was partly motivated by the need for an improved theory of the Auger process in solids. Indeed, due to the local character of the Auger transition, the key

solid-state quantity that enters the formulation for a filled electron band is the two-hole local density of states. Because of the presence of the Coulomb interaction and the extended character of valence states, the two-hole dynamics in the CVV Auger final state reflects the competition between localized and itinerant behavior. The CST of the Auger line shapes in solids is based on Anderson-like or Hubbard Hamiltonians, which retain only the on-site (repulsive) Coulomb term U. Depending on the U/W ratio, where W is the bandwidth, the typology of spectra can range from a featureless one (bandlike spectra), to a sharply featured one (atomiclike spectra). In any case, U determines the Auger line shape and the energy position of the spectral features simultaneously. Input data of the theory include the noninteracting (U=0) local densities of states. These can be obtained from self-consistent band structure calculations. Atomic multiplets and matrix elements are often adequate; the solid-state screening is introduced by reducing the F_0 Slater integral, while the other Slater integrals remain essentially unscreened in many systems like transition metals. One can compute Coulomb self-energies in solids reliably by standard methods; however, most authors treat the screened F_0 value as the only adjustable parameter of the theory. Since the band is degenerate, matrix Green's functions are necessary and we can build them from their noninteracting counterparts in the intermediate coupling scheme to allow for spin-orbit and Coulomb interactions; in addition, angular momentum is relaxed by crystal field effects. However, in many simple cases, crystal field effects are small, the *LSJ* quantum numbers apply, and to a good approximation the line shape is a superposition of independent *LSJ* components. In the present work, we adopt the same view. Therefore the following treatment is intended for each multiplet component separately: several spectra have been successfully interpreted in this way. Thus, for example, the dominant intensity in the Au and Ag spectra is given by the $^1G_4$ term, while the $^1S_0$ component is the most atomiclike in character, i.e., the highest U(*LSJ*) interaction term pertains to it.

Recent high-resolution experiments on Au (Ref. 15) and Ag (Ref. 20) noble metals, however, have shown that the CST framework must be refined. The unexpected result was that if we determine F_0 by optimizing the line shape, we do find a quite good one, but there is an essentially rigid energy shift between theory and experiment; on the other hand, by varying F_0, one easily removes the shift, but at the cost of a clear worsening of the profile. For Au (Ref. 15) the shift is about 1.2 eV. For Ag, the situation is similar (although the best fit of the Ag Auger line shape is not as good as the one for Au) and a shift of about 2.0 eV (Ref. 20) clearly results.

The root of the trouble was identified[16,17] in the neglect of the off-site interaction terms in the CST. This implied that an EHM description would resolve the discrepancy with experiment. Short of an exact solution at the time, we used a perturbational approach, valid for a small off-site interaction. The neat effect of the off-site terms was to provide an approximately rigid shift of the line shape,[16,17] thus supporting the above interpretation.

We are now in a position to analyze the problem with the exact solution, without being limited to small enough off-site terms. Also, the present approach, based on a Green's function formalism from the start (compare with Refs. 16 and 17), lends itself to an analytic extension to the multiple-band case. In the following, for both Ag and Au, we will discuss only the U($^1G_4$), U($^1S_0$) terms, as representative of the whole multiplet structure U(*LSJ*).

In Table II, we report the U and u values in units of $2\mathcal{V}$ used in our simulations and the U values in eV (in parentheses). The letters in bold show the correspondence between the entries of Table II and the panels in Fig. 3. The numerical values U,u in Tables I and II are the same: in fact we choose them having in mind the present discussion of Auger spectra. The U values give the same U/W ratios for our model as in the real Ag,Au metals; this is done for both $^1G_4$,$^1S_0$ components. The on-site values in eV for the real Au and Ag metals were taken from the literature.[15,20] In principle, refined U values should be determined by fitting the present theory with the actual crystal structure to the experiments; however, the current U(*LSJ*) are quite adequate for the present purpose, that is, to highlight the qualitative effects of the off-site interactions. Similarly, a realistic calculation of u is outside our immediate scope, and the values we use are readily obtained as a rough but reasonable estimate from the known lattice parameters and Thomas-Fermi screening. That the energy differences between multiplet terms are very well predicted by the CST suggests that the off-site interactions should be almost independent of the *LSJ* component. However, the bandwidth is different for silver and gold, which gives different U/W and u/W ratios for the two metals.

In Fig. 3, we compare the dispersionless limit of the exact solution with the CST in the local version: the dispersionless limit results are the same as in Fig. 2, where they

TABLE II. CVV Auger spectra of Au and Ag and the correspondence between U($^1G_4$), U($^1S_0$), u values, and panels in Fig. 3 (the correspondence is established by the entries in bold characters). The actual value of U model parameters (given in units of $2\mathcal{V}$, where $\mathcal{V}$ is the hopping term) is fixed by the U(*LSJ*) values in eV as shown in parentheses and taken from Refs. 14 and 20. The conversion factor to/from eV is given by the ratio of experimental (in eV) and model bandwidths. For the u model values, see discussion in the main text.

	$^1G_4$		$^1S_0$	
	U	u	U	u
Au	5.46 (5.2 eV)	2.84 [3(a)]	9.67 (9.2 eV)	2.84 [3(b)]
Ag	9.74 (5.6 eV)	4.7 [3(c)]	14.96 (8.6 eV)	4.7 [3(d)]

compare favorably with the exact EHM solution. The Lorentzian broadening is $\Gamma=0.6$, which in our units accounts well for the usual phenomenological broadening of the theoretical Auger line shape. Figures 3(a) and 3(b) model the effect of off-site interactions for Au. To estimate the energy shift, the U value in the (dotted) CST curve was determined to give the best fit of the dispersionless limit profile. The best CST fits are obtained at lower U values than those in Table II. The energy shifts obtained in this way are in good agreement with those obtained comparing CST to experiment. For Ag, Figs. 3(c) and 3(d), a similar energy shift between dispersionless limit and CST is found. For both Ag and Au, the search of the best CST fit gives consistent values of the energy shifts for the two *LSJ* terms. In summary, the overall effect of off-site interactions is twofold: (a) an energy shift between the two-particle local density of states as calculated in the present theory and the CST Auger line shape, implying that the EHM provides the sought generalization of the CST to explain both line shapes and the absolute positions of spectra and (b) the line shape is also modified. In order to go beyond the present qualitative argument, a proper extension of this theory to degenerate bands is needed. Such a generalization is currently under way.

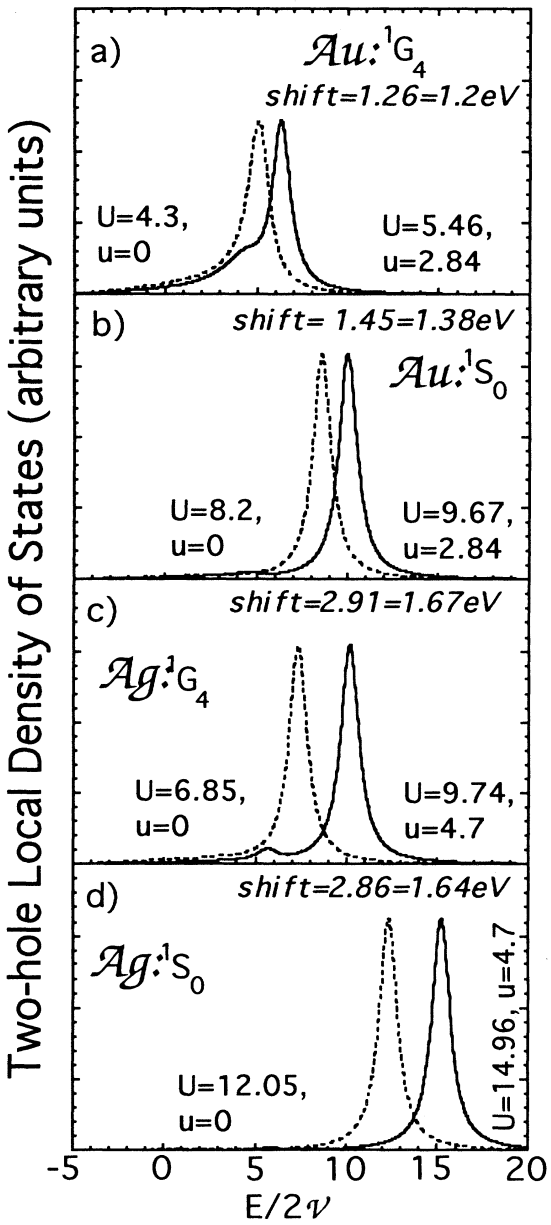

FIG. 3. Present ($U_{LSJ}\neq 0, u\neq 0$) and CST ($U_{LSJ}\neq 0, u=0$) theory for the Au, Ag, Auger CVV spectra; different *LSJ* terms are shown (see main text and Table II). Energy units are the same as in Figs. 1 and 2. The conversion to/from eV units is made with the help of Table II. For all panels (a)–(d): solid line is the present theory, dashed line is the CST theory. In all cases $\Gamma=0.6$, in good agreement with experimental values. In each panel, the energy shift between the present theory and CST line shape is calculated as the energy difference between the maxima of the two curves, when the CST is the best fit of the exact line shape. The best fit procedure also fixes the CST U value.

IV. CONCLUSIONS

We have proposed an exact Green's function solution for two particles on a lattice interacting with an arbitrary law $V(\mathbf{r})$. The method is valid for arbitrary dimensions and lattice structure, and generalizes the Kanamori solution for two particles in the Hubbard model. Two-body problems are usually dealt with by direct diagonalization of the Hamiltonian: the method shown here bypasses the eigenvalue problem and determines directly the two-particle propagators. Model calculations for a single-band simple cubic lattice with a Thomas-Fermi-like repulsive interaction demonstrate the practical usefulness of the approach. The general aspects of the solutions have been compared with the results of the Hubbard model and with the dispersionless or local limit of the theory. As a first application of the method to a physical situation, we examined how off-site interaction terms can modify the current theoretical description of the Auger decay in solids. By using a Thomas-Fermi-like potential, we have modeled the ^1G and ^1S components of the Au and Ag CVV line shapes, and the results support a previously proposed explanation of the energy shift between the CST and experiment. This explains the absolute energies of the experimental features. However, only minor changes in the line shapes are obtained, which is good, since the shapes already agreed well with experiment. However, these minor changes are qualitatively significant and, with other interparticle potentials $V(\mathbf{r})$, the present theory improves over the previous results both qualitatively and quantitatively. In general, one finds that the two-particle (or two-hole) resonance possesses an internal structure, leading to several (possibly infinitely many) bound states, instead of just one. The method is always more convenient than a direct diagonalization of the Hamiltonian, and is particularly suited for a short-ranged $V(r)$; for very long-ranged potentials, when direct inversion in the interaction cluster becomes difficult, we may consider perturbation-theory-based treatments of the long-distance tail of the interaction.

Besides, we are currently working out extensions of the present approach to multiple bands, in order to deal with a variety of problems.

APPENDIX

Equations (11) and (13), specialized to the local case of Eqs. (14), give a simple visualization of the concept of interaction cluster. In fact, let us define

$$\mathcal{V}^{Q}_{\mathbf{r}\mathbf{r}'}(z)=zV(\mathbf{r})g^{Q}_{\mathbf{r}\mathbf{r}'}(z) \tag{A1}$$

and introduce the effective Hamiltonian

$$\mathcal{H}^{Q}(z)=\sum_{\mathbf{r}\mathbf{r}'}\mathcal{V}^{Q}_{\mathbf{r}\mathbf{r}'}(z)|\mathbf{r}\rangle\langle\mathbf{r}'| \ . \tag{A2}$$

Then we can show that

$$G^{Q}_{00}(z)=[z\Gamma^{Q}_{\text{clust}}(00;z)-1]U^{-1} \ , \tag{A3}$$

where

$$\Gamma^{Q}_{\text{clust}}(00;z)=\langle\mathbf{r}=0|[z-\mathcal{H}^{Q}(z)]^{-1}|\mathbf{r}=0\rangle$$

$$=\frac{1}{z}\sum_{k=0}\left\langle 0\left|\left[\frac{\mathcal{H}^{Q}(z)}{z}\right]^{k}\right|0\right\rangle \tag{A4}$$

and $U=V(\mathbf{r}=0)$. Indeed, by expanding and using (A1), we get

$$\Gamma^{Q}_{\text{clust}}(00;z)=\frac{1}{z}[1+V_0G^{Q}_{00}(z)] \ , \tag{A5}$$

which is equivalent to (A3). Thus, by using a non-Hermitian effective Hamiltonian $\mathcal{H}^{Q}(z)$, we may reformulate the problem in such a way that the motion is confined in a cluster, whose size is fixed by the range of $V(\mathbf{r})$.

[1]J. Hubbard, Proc. R. Soc. London Ser. A **276**, 238 (1963).
[2]J. Kanamori, Prog. Theor. Phys. **30**, 275 (1963).
[3]C. M. Liegener, Phys. Rev. B **43**, 7561 (1991).
[4]O. Navarro and C. Wang, Solid State Commun. **83**, 473 (1992).
[5]J. Callaway and A. J. Hughes, Phys. Rev. **156**, 860 (1967).
[6]T. Hibma, G. A. Sawatzky, and J. Kommandeur, Chem. Phys. Lett. **23**, 21 (1973).
[7]For a short review, see, for example, M. Cini, Phys. Scr. **T41**, 59 (1992); or C. Verdozzi, in *(e,2e) and related processes, NATO Advanced Study Institute, Series B: Physics* (Kluwer, Dordrecht, 1993), p. 237.
[8]M. Cini, Solid State Commun. **20**, 605 (1976); **24**, 681 (1977).
[9]G. A. Sawatzky, Phys. Rev. Lett. **39**, 504 (1977).
[10]M. Cini, Surf. Sci. **87**, 483 (1979).
[11]P. W. Anderson, Phys. Rev. **124**, 41 (1961).
[12]M. Cini, Phys. Rev. B **17**, 2788 (1978).
[13]G. A. Sawatzky and A. Lenselink, Phys. Rev. B **21**, 1790 (1980).
[14]M. Cini and C. Verdozzi, J. Phys. Condens. Matter **1**, 7457 (1989).
[15]C. Verdozzi, M. Cini, J. F. McGilp, G. Mondio, D. Norman, J. A. Evans, A. D. Laine, P. S. Fowles, L. Duò, and P. Weightman, Phys. Rev. B **43**, 9550 (1991).
[16]C. Verdozzi, M. Cini, J. A. Evans, R. J. Cole, A. D. Laine, P. S. Fowles, L. Duò, and P. Weightman, Europhys. Lett. **16**, 743 (1991).
[17]M. Cini and C. Verdozzi, Phys. Scr. **T41**, 67 (1992).
[18]T. Morita, J. Phys. A **8**, 478 (1975).
[19]D. J. Chadi and M. L. Cohen, Phys. Rev. B **8**, 5747 (1973).
[20]R. J. Cole, C. Verdozzi, M. Cini, and P. Weightman, Phys. Rev. B **49**, 13 329 (1994).